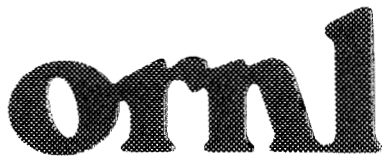




3 4456 0428503 9

ORNL/TM-13525



OAK RIDGE
NATIONAL
LABORATORY

LOCKHEED MARTIN 

Doppler Broadening Revisited

N. M. Larson
M. C. Moxon
L. C. Leal
H. Derrien

OAK RIDGE NATIONAL LABORATORY
CENTRAL RESEARCH LIBRARY
CIRCULATION SECTION
4500N ROOM 175

LIBRARY LOAN COPY

DO NOT TRANSFER TO ANOTHER PERSON
If you wish someone else to see this report, send in
name with report and the library will arrange a loan.

ORNL-118 (6-87)

MANAGED AND OPERATED BY
LOCKHEED MARTIN ENERGY RESEARCH CORPORATION
FOR THE UNITED STATES
DEPARTMENT OF ENERGY

This report has been reproduced directly from the best available copy.

Available to DOE and DOE contractors from the Office of Scientific and Technical Information, P.O. Box 62, Oak Ridge, TN 37831; prices available from (615) 576-8401, FTS 626-8401.

Available to the public from the National Technical Information Service, U.S. Department of Commerce, 5285 Port Royal Rd., Springfield, VA 22161.

This report was prepared as an account of work sponsored by an agency of the United States Government. Neither the United States Government nor any agency thereof, nor any of their employees, makes any warranty, express or implied, or assumes any legal liability or responsibility for the accuracy, completeness, or usefulness of any information, apparatus, product, or process disclosed, or represents that its use would not infringe privately owned rights. Reference herein to any specific commercial product, process, or service by trade name, trademark, manufacturer, or otherwise, does not necessarily constitute or imply its endorsement, recommendation, or favoring by the United States Government or any agency thereof. The views and opinions of authors expressed herein do not necessarily state or reflect those of the United States Government or any agency thereof.

ORNL/TM-13525

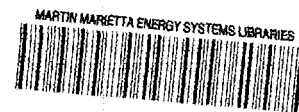
Computational Physics and Engineering Division

Doppler Broadening Revisited

N. M. Larson, M. C. Moxon, L. C. Leal, H. Derrien
Oak Ridge National Laboratory

Date Published: January 1998

Prepared by the
OAK RIDGE NATIONAL LABORATORY
managed by
LOCKHEED MARTIN ENERGY RESEARCH
for the
U.S. DEPARTMENT OF ENERGY
under contract DE-AC05-96OR22464



3 4456 0428503 9

CONTENTS

	<u>Page</u>
LIST OF FIGURES	v
ACKNOWLEDGMENTS	vii
ABSTRACT	ix
1. INTRODUCTION	1
2. DERIVATION OF DOPPLER BROADENING EQUATIONS	1
3. VERY NARROW RESONANCES	5
3.1 THEORETICAL DERIVATION FOR DELTA-FUNCTION RESONANCE .	5
3.2 CALCULATIONS	7
4. OTHER ENERGY-DEPENDENT CROSS SECTIONS	12
4.1 DOPPLER BROADENING OF $1/v$ CROSS SECTIONS	12
4.2 DOPPLER BROADENING OF A CONSTANT CROSS SECTION.	13
5. SUMMARY	15
6. REFERENCES	16
APPENDIX	17

LIST OF FIGURES

	<u>Page</u>
1. Direct comparison of the capture cross section (barns) broadened with the free gas model (solid line) and with the high energy Gaussian approximation (dashed line) for the 1-eV resonance of cesium.	8
2. Ratio of the Doppler-broadened capture cross section for cesium using the free gas model to that obtained using the high-energy Gaussian approximation	9
3. A small portion of the ^{235}U fission cross section.	10
4. Calculated FGM (solid) and HEGA (dashed) curves for the peak at 8.8 eV	11
A1. Relative peak position for the Doppler-broadened delta-function cross section as a function of temperature.	19

ACKNOWLEDGMENTS

This work was sponsored by the U.S. Department of Energy (DOE), under contract DE-AC05-84OR21400 with Lockheed Martin Energy Research. The authors are particularly indebted to D. Cabrilla, Environmental Management, U.S. Department of Energy, Washington, D.C., for his support.

ABSTRACT

The use of the high-energy Gaussian approximation to the free gas model of Doppler broadening has a long and distinguished history, dating back to early computer days when ψ and χ functions provided the most accurate computations available. In today's computing environment, however, use of the high-energy approximation is no longer necessary, and may lead to erroneous results. In this paper a derivation of the free gas model is presented, and the high-energy approximation derived from that. Differences between the two models are examined both analytically and via computations. Because the differences are visible (albeit not necessarily of significance in many cases), the authors recommend against continued use of the high-energy Gaussian approximation.

1. INTRODUCTION

Early in October of 1996, Mick Moxon and Herve Derrien began extended visits at Oak Ridge National Laboratory, working with L. Leal and N. Larson on various aspects of resonance parameter analysis. A major purpose of Moxon's visit was to facilitate comparisons between the two cross section analysis codes REFIT [MO77, MO91] and SAMMY [LA96], both in general and with particular emphasis on the ^{235}U analysis. As part of the comparison effort, REFIT and SAMMY calculations were made, first of the unbroadened ^{235}U cross sections and next of the Doppler-broadened cross sections, using parameters of the recent analysis of Leal, Derrien, and Larson [LE97]. Preliminary results are as follows:

For the unbroadened calculations, so long as all input parameters and all physical constants are given the exact same values for both codes, theoretical cross sections produced by the codes are equivalent to within 1 part in 10^6 (with certain exceptions). Detailed code comparison results will be described in another report [LA98].

During the course of the calculation minor glitches were found and fixed in each of the codes. In SAMMY, a too-short cutoff in the integration limits for the Doppler broadening was found to produce a slight discontinuity in the Doppler-broadened values at about 3.5 Doppler widths either side of a narrow resonance. In REFIT, a line of coding designed to prevent divide overflows when successive grid points were too close together led to miscalculation of the Doppler-broadened cross section for resonances with widths less than ~ 15 meV. For both codes the location and density of grid points used in the numerical integration schemes have been reconsidered and slightly restructured to optimize the calculations.

It is not the purpose of this paper to discuss either the details of the comparison nor any modifications made to the ^{235}U resonance parameter set as a result of this effort; rather, in this report we will concentrate on observations related to the Doppler broadening calculation.

Toward this end the remainder of this report is organized as follows: In Sect. 2 we present a derivation of the free gas model of Doppler broadening (sometimes referred to as the "ideal gas model"), and of the high-energy Gaussian approximation to the free gas model. In Sect. 3 the case of very narrow resonances is considered, first theoretically (assuming delta-function resonances) and then computationally. The Doppler broadening of various other energy-dependent cross sections is discussed in Sect. 4. A summary of results is presented in Sect. 5.

2. DERIVATION OF DOPPLER BROADENING EQUATIONS

The following is a quote (with notational changes for convenience) from Fritz Froehner's definitive paper "Applied Neutron Resonance Theory" [FR89]; comments in square brackets are added by the authors of this paper.

Doppler broadening is caused by thermal motion of the target nuclei. Consider a parallel beam of monoenergetic particles with lab velocity \vec{v} colliding with target nuclei whose velocities \vec{W} are distributed in such a way that $p(\vec{W}) d^3W$ is the fraction with velocities in a small three-dimensional region d^3W around \vec{W} . If ρ_1 and ρ_2 are the densities of beam and target particles, respectively, the number of reactions occurring per unit time and unit volume is

$$\rho_1 \rho_2 \int d^3W p(\vec{W}) |\vec{v} - \vec{W}| \sigma(m|\vec{v} - \vec{W}|^2/2) \equiv \rho_1 \rho_2 v \bar{\sigma}(mv^2/2) \quad , \quad (1)$$

where $\bar{\sigma}(mv^2/2)$ is the effective or Doppler-broadened cross section for incident particles with speed v [laboratory energy $mv^2/2$]. Obviously a $1/v$ cross section is not affected by Doppler broadening. Let us now assume that the target nuclei have the same velocity distribution as the atoms of an ideal [monatomic] gas, i.e. the Maxwell-Boltzmann distribution,

$$p(\vec{W}) d^3W = \frac{1}{\pi^{3/2} u^3} \exp\left(-\frac{W^2}{u^2}\right) \frac{d^3W}{u^3}, \quad \frac{M}{2} u^2 = kT, \quad (2)$$

where M is the nuclear mass and kT the gas temperature in energy units...

[End of quote from Froehner.]

Equation (1) is the direct result of the **definition** of the effective cross section for monoenergetic particles of mass m and energy E (laboratory velocity v). The effective cross section is given by the number of neutrons per unit volume, multiplied by the number of target nuclei per unit volume, times the probability that a reaction will occur per unit time at an energy equivalent to the relative velocity $|v - W|$, integrated over all values of W . As is shown in Sect. 4.1, the conservation of $1/v$ cross sections is a *consequence of the definition*, not a requirement “added on” to ensure compatibility with observed phenomena.

Equation (2) is the equation for the distribution of a free gas in three dimensions. Combining Eqs. (1) and (2), we find that

$$v \bar{\sigma}(mv^2/2) = \frac{1}{\pi^{3/2} u^3} \int_{\text{all } \vec{W}} d^3W \exp\left(-\frac{W^2}{u^2}\right) |\vec{v} - \vec{W}| \sigma(m|\vec{v} - \vec{W}|^2/2) \quad . \quad (3)$$

Changing the integration variable from \vec{W} to $\vec{w} = \vec{v} - \vec{W}$ and choosing spherical coordinates simplify the integral to the following:

$$\begin{aligned} v \bar{\sigma}\left(\frac{mv^2}{2}\right) &= \frac{1}{\pi^{3/2} u^3} \int_{\text{all } \vec{w}} d^3w \exp\left(-\frac{(v^2 - 2vw \cos \theta + w^2)}{u^2}\right) w \sigma\left(\frac{mw^2}{2}\right) \\ &= \frac{1}{\pi^{3/2} u^3} \int_0^\pi d\phi \int_0^\infty w^2 dw \int_0^\pi d(\cos(\theta)) \exp\left(-\frac{(v^2 - 2vw \cos \theta + w^2)}{u^2}\right) w \sigma\left(\frac{mw^2}{2}\right) \end{aligned}$$

$$\begin{aligned}
&= \frac{1}{\pi^{3/2} u^3} \int_0^{2\pi} d\phi \int_0^\infty dw w^3 \sigma\left(\frac{mw^2}{2}\right) \exp\left(-\frac{(v^2+w^2)}{u^2}\right) \int_{-1}^{+1} d\mu \exp\left(-\frac{2vw\mu}{u^2}\right) \\
&= \frac{2\pi}{\pi^{3/2} u^3} \int_0^\infty dw w^3 \sigma\left(\frac{mw^2}{2}\right) \exp\left(-\frac{(v^2+w^2)}{u^2}\right) \left(\frac{-u^2}{2vw}\right) \left[\exp\left(-\frac{2vw}{u^2}\right) - \exp\left(+\frac{2vw}{u^2}\right) \right] \\
&= \frac{1}{v\sqrt{\pi} u} \int_0^\infty dw w^2 \sigma\left(\frac{mw^2}{2}\right) \left[\exp\left(-\frac{(v-w)^2}{u^2}\right) - \exp\left(-\frac{(v+w)^2}{u^2}\right) \right]. \tag{4}
\end{aligned}$$

[This equation may be more familiar to most users when written as the sum of two integrals,

$$\begin{aligned}
\bar{\sigma}\left(E = \frac{mv^2}{2}\right) &= \frac{1}{v^2\sqrt{\pi} u} \int_0^\infty dw w^2 \sigma\left(\frac{mw^2}{2}\right) \exp\left(-\frac{(v-w)^2}{u^2}\right) \\
&\quad - \frac{1}{v^2\sqrt{\pi} u} \int_0^\infty dw w^2 \sigma\left(\frac{mw^2}{2}\right) \exp\left(-\frac{(v+w)^2}{u^2}\right). \tag{5}
\end{aligned}$$

At sufficiently high energies, the contribution from the second integral may be omitted since the value of the exponential is vanishingly small.]

To simplify Eq. (4) further, we make the following **definition**:

$$\begin{aligned}
s(w) &= \sigma(m(w)^2/2) \quad \text{for } w > 0 \\
&= -\sigma(m(-w)^2/2) \quad \text{for } w < 0. \tag{6}
\end{aligned}$$

Equation (4) then becomes

$$\bar{\sigma}\left(\frac{mv^2}{2}\right) = \frac{1}{v^2\sqrt{\pi} u} \int_{-\infty}^\infty dw w^2 s(w) \exp\left(-\frac{(v-w)^2}{u^2}\right). \tag{7}$$

For programming convenience, we make a change of variable from velocity to square root of energy. Thus instead of v we use

$$V = \sqrt{E} = v\sqrt{m/2}; \tag{8}$$

we redefine W to be

$$W = w\sqrt{m/2}, \tag{9}$$

and define U as

$$U = \sqrt{m/2} u = \sqrt{mkT/M}. \tag{10}$$

In addition, $S(W)$ is set equal to $s(w)$, or

$$\begin{aligned} S(W) &= \sigma((W)^2) && \text{for } W > 0 \\ &= -\sigma((-W)^2) && \text{for } W < 0 . \end{aligned} \quad (11)$$

These changes give the formulation which is used in SAMMY for the exact monatomic free gas model (FGM):

$$\bar{\sigma}(V^2) = \frac{1}{V^2 \sqrt{\pi} U} \int_{-\infty}^{\infty} dW W^2 S(W) \exp\left(-\frac{(V-W)^2}{U^2}\right) . \quad (12)$$

This method is described in Revision 3 of the SAMMY manual [LA96, page 92q; note however the typographical error in Eq. (IVF.4), in which u should be squared]. Implementation of a routine based on Eq. (7 or 12) within the newest version of REFIT has decreased the time required for the calculation below a few eV; older versions of REFIT use the free gas model only at low energies and the high-energy Gaussian approximation at higher energies. [Users of older versions of REFIT should be aware of a center-of-mass conversion error affecting the exact free gas model, for low-mass nuclei. Another error, related to integration near $w = 0$ in Eq. (4 or 5), affected only very-low-energy cross sections. Both errors have been corrected in the newest version of the code, which is available from the author.]

Note that, either in the form of Eq. (4 or 5) or in the form of Eq. (7 or 12), this is the correct equation for all monatomic free gas Doppler broadening, no matter what the energy-dependence of the cross section. These equations hold for $1/\nu$ cross sections, for constant cross sections, and for cross sections with resonance structure.

To transform to the high-energy Gaussian approximation (hereafter referred to as HEGA) from the FGM, define E as V^2 and E' as W^2 . Then Eq. (12) takes the form

$$\begin{aligned} \bar{\sigma}(E) &\cong \frac{1}{E \sqrt{\pi} U} \int_{E_{min} > 0}^{\infty} \frac{dE'}{2\sqrt{E'}} E' \sigma(E') \exp\left(-\frac{(\sqrt{E}-\sqrt{E'})^2}{U^2}\right) \\ &= \frac{1}{\sqrt{\pi} \Delta} \int_{E_{min}}^{\infty} dE' \sqrt{\frac{E'}{E}} \sigma(E') \exp\left(-\frac{4(E-\sqrt{EE'})^2}{\Delta^2}\right) . \end{aligned} \quad (13)$$

in which the lower limit has been changed from $-\infty$ to E_{min} , a number above zero, since the next step involves approximations which are valid only for $E' \gg 0$. The quantity Δ^2 in Eq. (13) is defined as

$$\Delta^2 = U^2 / 4 E ; \quad (14)$$

note that this quantity is energy-dependent. Expanding the integrand of Eq. (13) in powers of $(E-E')$, and keeping only first-order terms, give a value of 1 for the ratio E'/E , and $E - E - (E-E')/2 = (E-E')/2$ for the quantity in the exponential. Thus the HEGA becomes

$$\bar{\sigma}_{HEGA}(E) \approx \frac{1}{\sqrt{\pi} \Delta} \int_{E_{min}}^{\infty} dE' \sigma(E') \exp\left(-\frac{(E-E')^2}{\Delta^2}\right). \quad (15)$$

Extending the lower limit to negative infinity (since that portion of the integrand is essentially zero) then gives the usual Gaussian formulation of the free gas model.

3. VERY NARROW RESONANCES

3.1. THEORETICAL DERIVATION FOR DELTA-FUNCTION RESONANCE

In order to understand whether HEGA might differ from FGM even at high energies, consider first the case of an isolated narrow resonance. For illustrative purposes the cross section is taken to be a delta-function of the form

$$\sigma(E') = \delta(E' - E_0). \quad (16)$$

With this value for the cross section, the HEGA-broadened cross section is found directly from Eq. (15):

$$\bar{\sigma}_{HEGA}(E) = \frac{1}{\sqrt{\pi} \Delta} \exp\left(-\frac{(E-E_0)^2}{\Delta^2}\right) = \frac{1}{\sqrt{\pi} 2 UV} \exp\left(-\frac{(V^2 - V_0^2)^2}{4 V^2 U^2}\right), \quad (17)$$

in which the energy-variables have been translated to square-root-of-energy variables for ease of comparison with the FGM, and E_0 is set equal to V_0^2 . To evaluate the FGM cross section, the integration variable W in Eq. (11) is first replaced by variable $E' = W^2$, so that

$$\begin{aligned} \bar{\sigma}_{FGM}(E) &= \frac{1}{V^2 \sqrt{\pi} U} \int_{-\infty}^{\infty} \frac{dE'}{2\sqrt{E'}} E' \delta(E' - E_0) \exp\left(-\frac{(V-\sqrt{E'})^2}{U^2}\right) \\ &= \frac{1}{V^2 \sqrt{\pi} U} \frac{\sqrt{E_0}}{2} \exp\left(-\frac{(V-\sqrt{E_0})^2}{U^2}\right) = \frac{1}{\sqrt{\pi} 2 UV} \frac{V_0}{V} \exp\left(-\frac{(V-V_0)^2}{U^2}\right). \end{aligned} \quad (18)$$

To compare Eq. (18) with Eq. (17) at the position of the resonance ($E = E_0$, or equivalently $V = V_0$), simply make those substitutions in the two equations. Values of the two expressions are exactly the same:

$$\bar{\sigma}_{FGM}(E = E_0) = \bar{\sigma}_{HEGA}(E = E_0) = \frac{1}{\sqrt{\pi} 2 U V_0} \quad (19)$$

To compare Eq. (18) with Eq. (17) at other energies, define F as the exponent (without the minus sign) for the free gas model, and H similarly as the exponent for the high energy Gaussian approximation. Set $x = V - V_0$. Then the exponents take the following values:

$$F = x^2 / U^2 \quad (20)$$

and

$$\begin{aligned} H &= \frac{(V^2 - V_0^2)^2}{4 V^2 U^2} = \frac{(V^2 - (V-x)^2)^2}{4 V^2 U^2} = \frac{(V^2 - V^2 + 2 Vx - x^2)^2}{4 V^2 U^2} \\ &= \frac{(2 Vx - x^2)^2}{4 V^2 U^2} = \frac{4 V^2 x^2 (1 - x/2V)^2}{4 V^2 U^2} = \frac{x^2}{U^2} \left(1 - \frac{x}{2V}\right)^2 \end{aligned} \quad (21)$$

In this form it is clear that positive x implies $F > H$, negative x implies $F < H$. It therefore follows that the exponential term for the FGM is larger than the exponential term for the HEGA when the energy E is less than the resonance energy E_0 , and smaller if greater. Since the other energy-dependent factors in the FGM and HEGA have similar properties, the relationship between the two broadened cross sections can be summarized as

$$\begin{aligned} \bar{\sigma}_{FGM}(E) &> \bar{\sigma}_{HEGA}(E) && \text{for } E < E_0 ; \\ \bar{\sigma}_{FGM}(E) &= \bar{\sigma}_{HEGA}(E) && \text{for } E = E_0 ; \\ \bar{\sigma}_{FGM}(E) &< \bar{\sigma}_{HEGA}(E) && \text{for } E > E_0 . \end{aligned} \quad (22)$$

It is also possible to show, by setting the derivatives with respect to the velocity V equal to zero, that the position of the broadened peak is characterized by a slight shift to the higher energy for the HEGA when compared to the more accurate FGM. Details are presented in the appendix.

3.2. CALCULATIONS

To verify the results described above for delta-function resonances, calculations were performed with SAMMY using an invented element of mass 10.000 amu, ground state spin 0, with 12 s-wave resonances located at energies (in eV) of 0.25, 0.5, 1.0, 2.0, 5.0, 10.0, 20.0, 50.0, 100.0, 200.0, 500.0, and 1000.0. The radiation width for each resonance was set at 1.0 meV, and the neutron width and two fission widths for each resonance were 0.5 meV. This “element” was designated “resium” by John Story [ST81].

The same calculations have also been performed with REFIT, as well as with the codes NJOY [MA94] and MULTIPOLE [HW87]; results will be reported elsewhere [LA98].

Figure 1 shows the FGM and the HEGA for the resonance at 1 eV. Differences between the two are clearly visible on the plot. Fig. 2 gives the ratio of FGM to HEGA for the energy range from $\sim 10^{-4}$ to 1.2 keV. As expected, the magnitude of this ratio becomes closer to unity as energy increases; nevertheless the differences between the two methods are still quite pronounced even for the 20-eV resonance.

Careful examination shows that physical resonances exhibit the same kinds of behavior, although for most resonances the differences between HEGA and FGM are smaller than the experimental uncertainties. One example is given in Fig. 3a, which represents a small portion of the ^{235}U fission cross section; Fig. 3b shows the resonance (doublet) near 8.8 eV. The calculated HEGA and FGM curves for the uppermost portion of this peak have been redrawn in Fig. 4 (with a dense grid, to ensure that the picture is visually smooth).

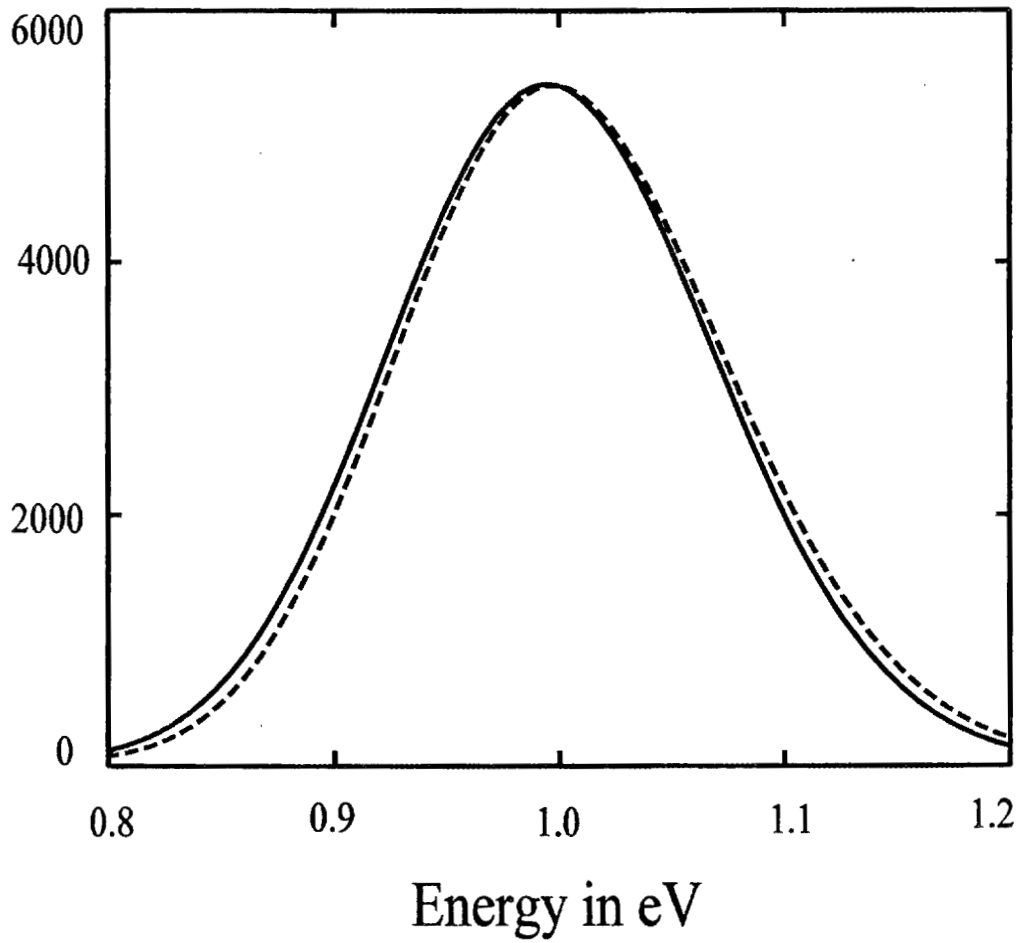


Figure 1. Direct comparison of the capture cross section (barns) broadened with the free gas model (solid line) and with the high energy Gaussian approximation (dashed line) for the 1-eV resonance of resium.

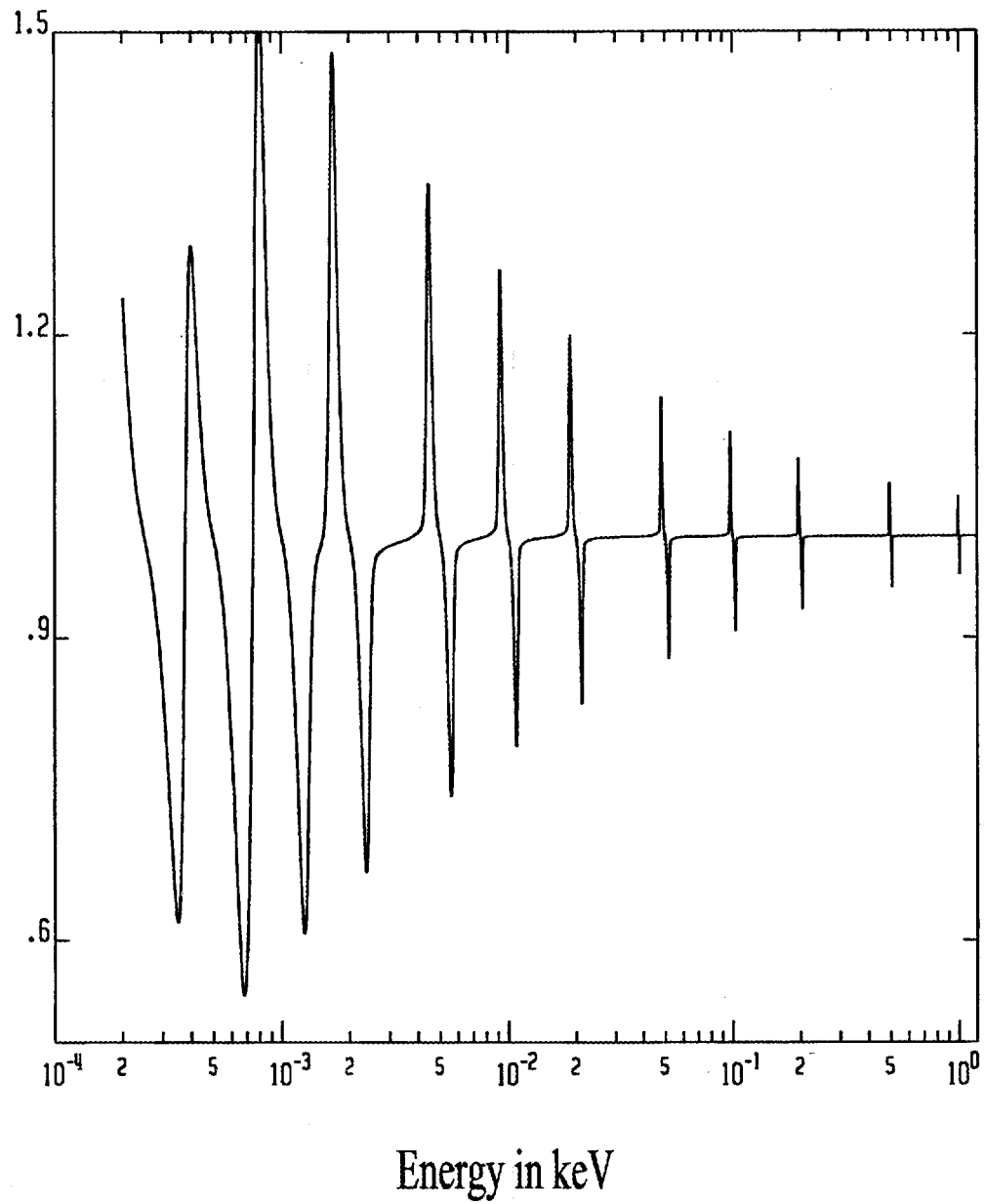


Figure 2. Ratio of the Doppler broadened capture cross section for Resium using the free gas model to that obtained using the high energy Gaussian approximation.

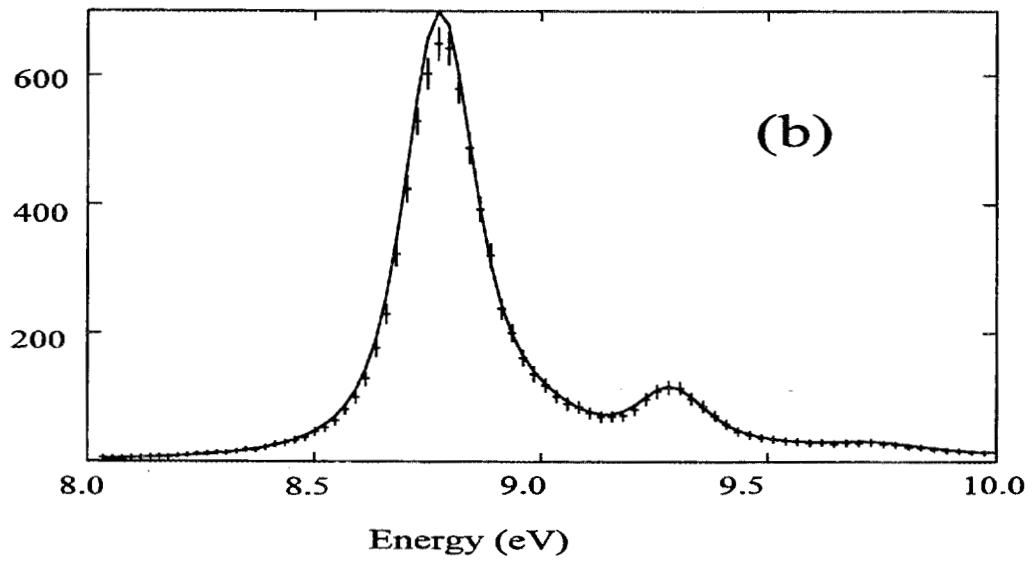
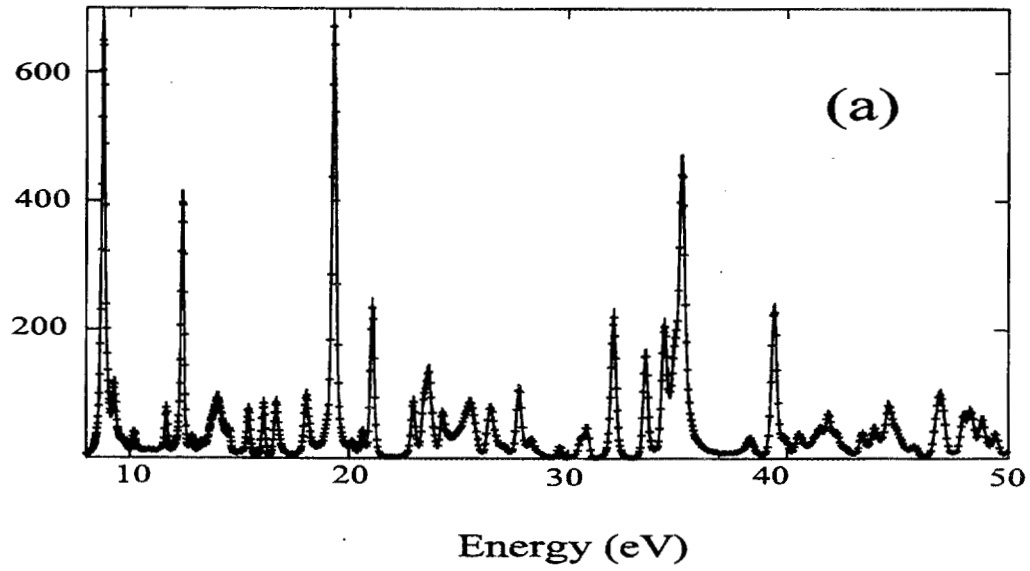


Figure 3. A small portion of the ^{235}U fission cross section. Part (a) shows experimental data (crosses) and preliminary FGM fit (solid line). The curve from 8 to 10 eV is shown in more detail in Part (b) of the figure. On the scale used for these plots, the HEGA calculation is indistinguishable from the FGM.

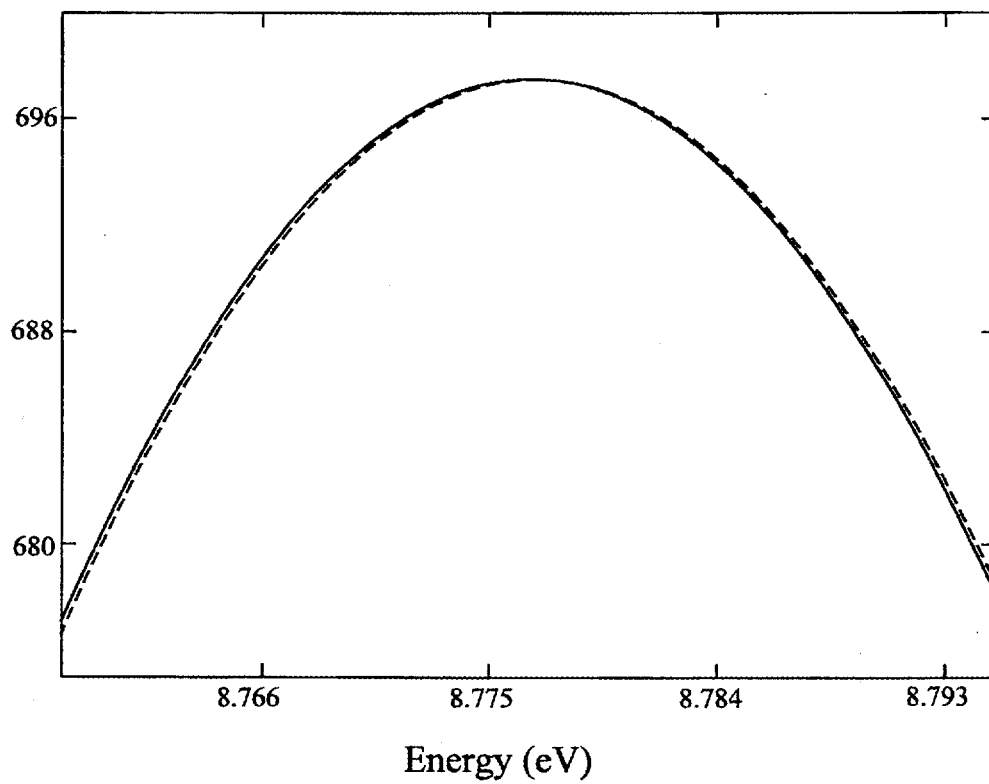


Figure 4. Calculated FGM (solid) and HEGA (dashed) curves for the peak at 8.8 eV.

4. OTHER ENERGY-DEPENDENT CROSS SECTIONS

No discussion of Doppler broadening would be complete without an analysis of the effects of Doppler broadening on particular types of cross sections. Here we examine two important types of energy-dependencies: First, the $1/v$ cross section is considered analytically via both FGM and HEGA. Second, analytical integration is used to determine FGM- and HEGA-broadened constant cross sections.

4.1 DOPPLER BROADENING OF $1/v$ CROSS SECTIONS

Doppler broadening is expected to preserve (i.e., leave unchanged) a $1/v$ -cross section. To test whether this is the case with FGM and/or HEGA broadening, we note that a $1/v$ -cross section may be expressed as

$$\sigma(W^2) = \frac{\sigma_0 V_0}{W} , \quad (23)$$

where the subscript “0” denotes constants. To evaluate the FGM with this type of cross section, note that our function S of Eq. (10), combined with Eq. (23), gives

$$\begin{aligned} S(W) &= \frac{\sigma_0 V_0}{W} \quad \text{for } W \geq 0 \\ &= -\frac{\sigma_0 V_0}{-W} = \frac{\sigma_0 V_0}{W} \quad \text{for } W < 0 . \end{aligned} \quad (24)$$

From Eq. (11) the FGM-broadened form of the $1/v$ cross section is therefore

$$\bar{\sigma}(V^2) = \frac{\sigma_0 V_0}{V^2 \sqrt{\pi} U} \int_{-\infty}^{+\infty} W dW e^{-(V-W)^2/U^2} = \frac{\sigma_0 V_0}{V} , \quad (25)$$

i.e., in the exact same mathematical form as the original of Eq. (22). In other words, a $1/v$ cross section is conserved under Doppler broadening with the free gas model.

That is not the case for HEGA broadening. With the HEGA of Eq. (14) (with lower limit of $-\infty$), the Doppler-broadened $1/v$ cross section takes the form

$$\bar{\sigma}_{HEGA}(E) = \frac{1}{\sqrt{\pi} \Delta} \int_{-\infty}^{+\infty} dE' \frac{\sigma_0 V_0}{\sqrt{E'}} e^{-(E-E')^2/\Delta^2} = \frac{\sigma_0 V_0}{\sqrt{\pi} \Delta} \int_{-\infty}^{+\infty} \frac{dE'}{\sqrt{E'}} e^{-(E-E')^2/\Delta^2} , \quad (26)$$

which is not readily integrable analytically. What is clear is that the result is *not* $1/v$.

4.2. DOPPLER BROADENING OF A CONSTANT CROSS SECTION.

In contrast to the $1/v$ cross section, a constant cross section is not conserved under Doppler broadening. That is true experimentally can be seen by examining very low energy capture cross sections, for which the unbroadened cross section is constant (which can be shown by taking the low-energy limit of the Reich-Moore equations, e.g.) but the experimental cross section rises with decreasing energy. See, for example, the S elastic cross section from 0.01 to 1.0 eV or the Cu elastic cross section below 2.0 eV (on pages 100 and 234, respectively, of [VM88]), which clearly rise with decreasing energy.

To calculate analytically what effect FGM and HEGA broadening have upon a constant cross section, we first note that a constant cross section can be expressed as

$$\sigma(E) = \sigma_0 . \quad (27)$$

The function S needed for our formulation of FGM broadening (see Eq. (10)) is found to be

$$\begin{aligned} S(W) &= \sigma_0 \text{ for } W \geq 0 \\ &= -\sigma_0 \text{ for } W < 0 , \end{aligned} \quad (28)$$

so that Eq. (11) gives, for the FGM-broadened constant cross section,

$$\bar{\sigma}(V^2) = \frac{\sigma_0}{V^2 \sqrt{\pi} U} \left[\int_0^{\infty} dW W^2 e^{-(V-W)^2/U^2} - \int_{-\infty}^0 dW W^2 e^{-(V-W)^2/U^2} \right] . \quad (29)$$

Replacing $(W-V)/U$ by x gives

$$\begin{aligned} \bar{\sigma}(V^2) &= \frac{\sigma_0 U^3}{V^2 \sqrt{\pi} U} \left[\int_{-v}^{\infty} dx (x^2 + 2xv + v^2) e^{-x^2} - \int_{-\infty}^{-v} dx (x^2 + 2xv + v^2) e^{-x^2} \right] \\ &= \frac{\sigma_0}{v^2 \sqrt{\pi}} \left[\int_0^{\infty} + \int_{-v}^0 - \int_{-\infty}^0 + \int_{-v}^0 \right] dx (x^2 + 2xv + v^2) e^{-x^2} \end{aligned}$$

$$\begin{aligned}
&= \frac{\sigma_0}{v^2 \sqrt{\pi}} \left[2 \int_0^\infty dx (2xv) e^{-x^2} + 2 \int_{-v}^0 dx (x^2 + 2xv + v^2) e^{-x^2} \right] \\
&= \frac{\sigma_0 4v}{v^2 \sqrt{\pi}} \int_0^\infty dx e^{-x^2} + \frac{2\sigma_0}{v^2 \sqrt{\pi}} \int_{-v}^0 x^2 dx e^{-x^2} \\
&\quad + \frac{4v\sigma_0}{v^2 \sqrt{\pi}} \int_{-v}^0 dx e^{-x^2} + \frac{2\sigma_0 v^2}{v^2 \sqrt{\pi}} \int_{-v}^0 dx e^{-x^2} \\
&= \frac{\sigma_0 4}{v \sqrt{\pi}} \frac{1}{2} + \frac{2\sigma_0}{v^2 \sqrt{\pi}} \left(-\frac{v}{2} e^{-v^2} + \frac{\sqrt{\pi}}{4} [\operatorname{erfc}(0) - \operatorname{erfc}(v)] \right) \\
&\quad + \frac{4\sigma_0}{v \sqrt{\pi}} \left(-\frac{1}{2} [1 - e^{-v^2}] \right) + \frac{2\sigma_0}{\sqrt{\pi}} [\operatorname{erfc}(0) - \operatorname{erfc}(v)] \\
&= \frac{\sigma_0}{v \sqrt{\pi}} e^{-v^2} + \sigma_0 \left(\frac{1}{2v^2} + 1 \right) \left(1 - \operatorname{erfc}(v) \right) , \tag{30}
\end{aligned}$$

in which we have replaced V/U by v .

In the limit of small v , the quantity in Eq. (30) becomes

$$\bar{\sigma}(V^2) \rightarrow \sigma_0 \left[\frac{1}{\sqrt{\pi} v} + \frac{1}{2v^2} \frac{2}{\sqrt{\pi}} (v + v^3) \right] \rightarrow \frac{\sigma_0}{\sqrt{\pi} v} , \tag{31}$$

so that the leading term is $1/v$; this is somewhat counterintuitive but is nevertheless observed in measured low-energy cross sections. For large values of v , the limiting case is

$$\bar{\sigma}(V^2) \rightarrow \sigma_0 \left[0 + 1 \times 1 \right] \rightarrow \sigma_0 , \tag{32}$$

i.e., the broadened cross section is a constant, as expected.

In contrast, HEGA broadening preserves a constant cross section everywhere:

$$\bar{\sigma}_{HEGA}(E) = \frac{\sigma_0}{\sqrt{\pi} \Delta} \int_{-\infty}^{\infty} dE' e^{-(E-E')^2/\Delta^2} = \sigma_0 ; \quad (33)$$

that is, the Gaussian kernel is normalized to unity, as expected. This result, which may intuitively appear to be correct, is nevertheless unphysical. As discussed above, It is well known that measured (and therefore Doppler-broadened) cross sections exhibit $1/v$ behavior at very low energies.

5. SUMMARY

The free gas model of Doppler broadening appears to be a reasonable approximation for most solid samples for neutron energy above a few tens of eV, where solid state effects can be neglected. One of the problems is the determination of the effective temperature of the sample, which should be obtained from Lamb equation (LA39) relating the effective temperature to the Debye temperature and to the actual temperature of the sample. The Debye temperature is not always well known, and most experimenters have not monitored the sample temperature during measurement, particularly for measurements performed with samples at low temperature (e.g., liquid nitrogen temperature). Consequently the effective temperature should be one of the variables to be determined in the fit; both SAMMY and REFIT permit this option.

In this paper we have described comparisons, both theoretical and computational, of Doppler broadening using the “exact” free gas model vs. Doppler broadening using the customary high-energy Gaussian approximation. These comparisons indicate clearly that the approximate formulation does not provide an accurate representation of the exact free gas model, even for relatively high energies. While differences between the exact and the approximate models are generally small for physical resonances, nevertheless those differences do persist at all energies.

Early codes for resonance analysis and evaluation generally used the Gaussian approximation, because the ψ and χ functions (results of the convolution of the Gaussian function and the Breit-Wigner shape of the resonances) were well known and tabulated (saving computer time and space). Today, more sophisticated (and more accurate) formalisms are used for the calculation of the cross sections; the ψ and χ functions cannot be used for the Doppler broadening with these formalisms. Hence, there is no longer any computational advantage to using the Gaussian approximation.

Use of the approximate HEGA model (the high-energy Gaussian approximation) is therefore discouraged.

REFERENCES

- FR89 F. H. Fröhner, "Applied Theory of Resolved and Unresolved Resonances," *Applied Nuclear Theory and Nuclear Model Calculations for Nuclear Technology Applications*, M.K. Mehta and J.J. Schmidt (eds.), World Scientific, Singapore (1989), p. 170.
- HW87 R. Hwang, *Nucl. Sci. and Eng.* **96** (1987) 192.
- LA39 W. E. Lamb, *Phys. Rev.* **55** (1939) 190.
- LA96 N. M. Larson, *Updated User Guide for SAMMY: Multilevel R-matrix Fits to Neutron Data Using Bayes' Equations*, ORNL/TM-9179, Martin Marietta Energy Systems, Inc., Oak Ridge National Laboratory (August 1984); see also ORNL/TM-9179/R1 (July 85), /R2 (June 1989) and /R3 (September 1996).
- LA98 N. M. Larson et al., to be published.
- LE97 L. C. Leal, H. Derrien, N. M. Larson, and R. Q. Wright, *R-Matrix Analysis of ^{235}U Neutron Transmission and Cross Sections in the Energy Range 0 to 2.25 keV*, to be published as ORNL/TM-13516, Martin Marietta Energy Systems, Inc., Oak Ridge National Laboratory (November 1997).
- MA94 R. E. MacFarlane and D. W. Muir, "The NJOY Nuclear Data Processing System, Version 91," LA-12740-M, Los Alamos National Lab. (April 1994).
- MO77 M. C. Moxon, "REFIT, a least squares fitting program for resonance analysis of neutron transmission and capture data," *Neutron data for structural Materials for Fast Reactors*, Pergamom Press (1977) 644.
- MO91 M. C. Moxon, "REFIT, A Least Squares Fitting Program for Resonance Analysis of Neutron Transmission and Capture Data," AEA-Intec-0470 (April 1991).
- ST81 J. Story, private communication, 1981.
- VM88 V. McLane, C. L. Dunford, P. F. Rose, *Neutron Cross Sections, Volume 2, Neutron Cross Section Curves*, Academic Press, Inc., San Diego, CA (1988).

APPENDIX. POSITION OF PEAK OF DOPPLER-BROADENED CROSS SECTION

The HEGA- and FGM-broadened cross sections for very narrow (delta-function) resonances were discussed in Sect. 3.1 of this report; exact expressions for the two quantities are shown in Eqs. (16) and (17) respectively. In this appendix we derive the expressions for the exact energy-value of the peak cross section, where “peak” is assumed to mean “highest value of the function.” This location occurs at that energy (or, equivalently, that value of V) at which the derivative of the function is zero.

For the HEGA cross section, the derivative of Eq. (16) with respect to “velocity” V is given by

$$\begin{aligned} \frac{\partial}{\partial V} \bar{\sigma}_{HEGA} &= \bar{\sigma}_{HEGA} \times \left(-\frac{1}{V} - \frac{2V2(V^2 - V_0^2)}{4V^2 U^2} - \frac{2}{V} \frac{(V^2 - V_0^2)^2}{4V^2 U^2} \right) \\ &= -\frac{\bar{\sigma}_{HEGA}}{2V^3 U^2} (V^4 + 2V^2 U^2 - V_0^4) . \end{aligned} \quad (\text{A.1})$$

Let $E_{Hp} = V_{Hp}^2$ represent the position of the peak. Setting the derivative in Eq. (A.1) equal to zero gives

$$V_{Hp}^4 + 2V_{Hp}^2 U^2 - V_0^4 = 0 , \quad (\text{A.2})$$

which has the solution

$$E_{Hp} = V_{Hp}^2 = \sqrt{V_0^4 + U^4} - U^2 . \quad (\text{A.3})$$

To simplify this equation a bit more, variable X is defined as

$$X = U^2 / V_0^2 ; \quad (\text{A.4})$$

with this definition Eq. (A.3) takes the form

$$Y_H = E_{Hp} / V_0^2 = E_{Hp} / E_0 = \sqrt{1 + X^2} - X , \quad (\text{A.5})$$

in which Y_H is defined as the ratio shown.

For the FGM cross section, the derivative of Eq. (17) with respect to V is given by

$$\begin{aligned} \frac{\partial}{\partial V} \bar{\sigma}_{FGM} &= \bar{\sigma}_{FGM} \times \left(-\frac{2}{V} - \frac{2(V-V_0)}{U^2} \right) \\ &= -\bar{\sigma}_{FGM} \times \frac{2}{VU^2} (U^2 + V^2 - VV_0) . \end{aligned} \quad (\text{A.6})$$

Setting this to zero at the position of the peak ($E_{Fp} = V_{Fp}^2$) gives

$$U^2 + V_{Fp}^2 - V_{Fp} V_0 = 0 , \quad (\text{A.7})$$

which, for $V_0 \geq 4U$, has the solution

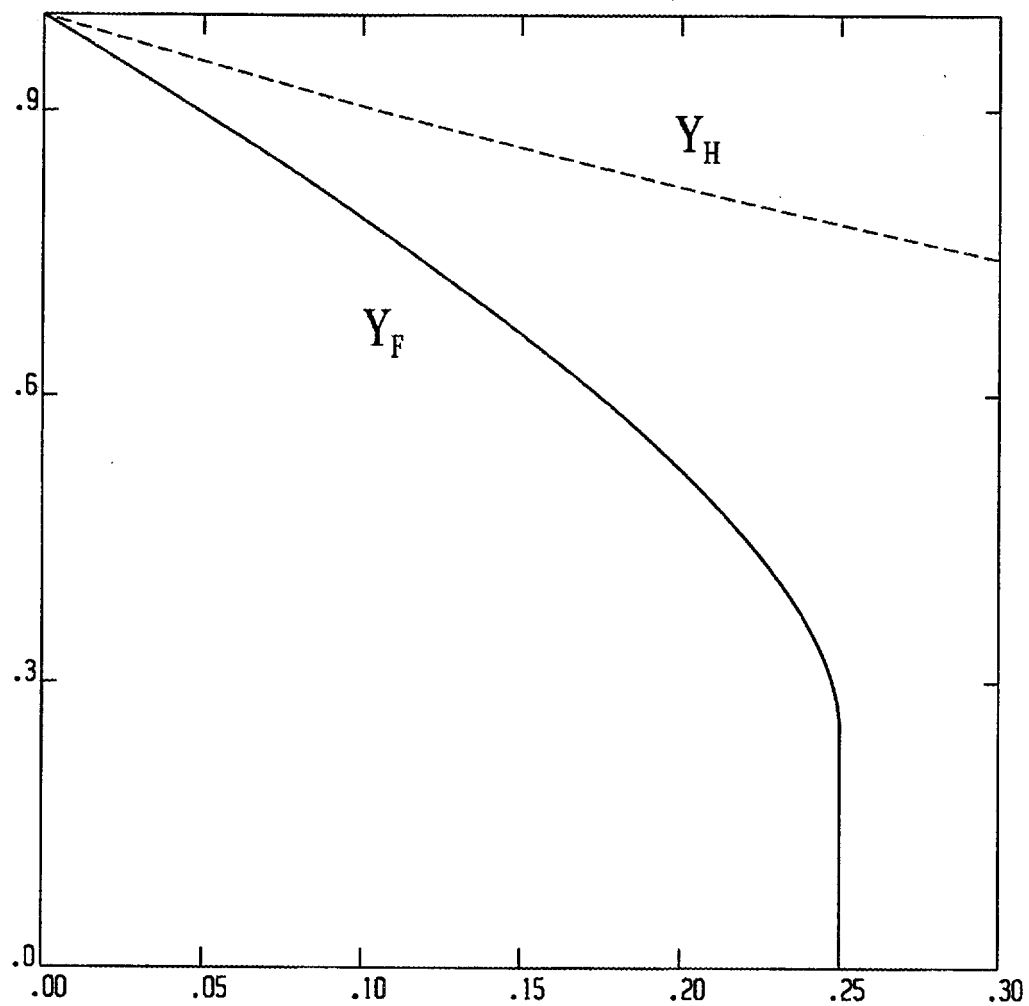
$$V_{Fp} = \frac{1}{2} \left(V_0 + \sqrt{V_0^2 - 4U^2} \right) . \quad (\text{A.8})$$

Squaring this expression and using the definition of X from Eq. (A.4) give

$$Y_F = E_{Fp} / V_0^2 = E_{Fp} / E_0 = \frac{1}{4} \left(1 + \sqrt{1 - 4X} \right)^2 . \quad (\text{A.9})$$

Functions Y_H and Y_F are plotted as the dashed and solid curves, respectively, in Fig. A1; note that the x -axis is directly proportional to temperature T . On this plot, the value $Y = 1$ corresponds to the position of the unbroadened peak. For both versions of Doppler broadening, the position of the Doppler-broadened peak is lower than the position of the unbroadened peak; further, the position of the peak with FGM broadening is lower than that of the HEGA broadening.

Calculations with REFIT involving the 6.7-eV resonance of U238 essentially substantiate this temperature-dependence of the peak position. The position of the peak at room temperature is approximately 40 meV higher than the position of the peak at 20 times room temperature.



$$X = U^2 / V_0^2 = m k T / (M E_0)$$

Fig. A1. Relative peak position for the Doppler-broadened delta-function cross section as a function of temperature. The solid curve shows the free gas model, and the dashed the high-energy Gaussian approximation.

INTERNAL DISTRIBUTION

- | | |
|---------------------|--|
| 1. B. L. Broadhead | 23-27. L. C. Leal |
| 2-7. H. Derrien | 28. C. V. Parks |
| 8. F. C. Difilippo | 29. R. W. Roussin |
| 9. C. Y. Fu | 30. C. H. Shappert |
| 10. N. M. Greene | 31. M. S. Smith |
| 11. K. Guber | 32. R. R. Spencer |
| 12. J. A. Harvey | 33. R. M. Westfall |
| 13. C. M. Hopper | 34. J. E. White |
| 14. D. T. Ingersoll | 35. R. Q. Wright |
| 15. P. E. Koehler | 36. RSICC |
| 16. M. A. Kuliasha | 37-38. Laboratory Records for submission to OSTI |
| 17. D. C. Larson | 39. Laboratory Records, ORNL-RC |
| 18-22. N. M. Larson | 40. Central Research Library |

EXTERNAL DISTRIBUTION

41. P. Blaise, DER/SPRC/LEPH, Batiment 230, Centre d'Etudes de CADARACHE, 13108 Saint Paul-lez-Durance, France
42. R. Block, Gaerttner LINAC Laboratory, Department of Environmental and Energy Engineering, Rensselaer Polytechnic Institute, Troy, NY 12180-3590
43. O. Bouland, DER/SPRC/LEPH, Batiment 230, Centre d'Etudes de CADARACHE, 13108 Saint Paul-lez-Durance, France
44. J. Burke, Gaerttner LINAC Laboratory, Department of Environmental and Energy Engineering, Rensselaer Polytechnic Institute, Troy, NY 12180-3590
45. D. Cabrilla, U.S. Department of Energy, EM-66, Clover Leaf, Room 1199, 19901 Germantown Road, Germantown, MD 20874-1290
46. D. E. Carlson, Reactor and Plant System Branch, Division of System Research, Office of Nuclear Regulatory Research, U.S. Nuclear Regulatory Commission, MS T-10 G6, RM T-10, 17, Washington, DC 20555-0001
47. F. Corvi, Central Bureau for Nuclear Measurements, Steenweg op Retie, 2240 Geel, Belgium
48. D. E. Cullen, MS L-298, Lawrence Livermore National Laboratory, P. O. Box 808, Livermore, CA 94550
49. Y. Danon, Physics Department, NRCN, P. O. Box 9001, Beer-Sheva 84190, Israel
50. R. L. Dintaman, U.S. Department of Energy, DP-13, Washington, DC 20585
51. C. Dunford, Bldg 197D, National Nuclear Data Center, Brookhaven National Laboratory, Upton, NY 11973
52. J. R. Felty, U.S. Department of Energy, DP-311, Washington DC 20585
53. P. Finck, Argonne National Laboratory, Reactor Analysis Division, Bldg 208, Argonne, IL 60439
54. E. Fort, DER/SPRC/LEPH, Batiment 230, Centre d'Etudes de CADARACHE, 13108 Saint Paul-lez-Durance, France
55. C. M. Frankle, NIS-6, MS J562, Los Alamos National Laboratory, Los Alamos, NM 87545
56. S. C. Frankle, X-TM, MS B226, Los Alamos National Laboratory, Los Alamos, NM 87545
57. F. Froehner, Kernforschungszentrum Karlsruhe, Institut f. Neutronenphysik und Reaktorteknik, Postfach 336 40, D-76021 Karlsruhe, Germany
58. W. Furman, Frank Laboratory of Neutron Physics, JINR, Dubna, Russia

59. S. Ganesan, Head, Nuclear Data Section, Indira Gandhi Centre for Atomic Research, Kalpakkam 603 102, Tamilnadu, India
60. H. Gruppelaar, Netherlands Energy Research Foundation ECN, Westerduinweg 3, P. O. Box 1, NL 1755 ZG Petten, Netherlands
61. F. Gunsing, Centre D'Etudes De Saclay, F-Saclay - 91191 GIF-SUR-YVETTE Cedex, France
62. G. M. Hale, T-2, MS B243, Los Alamos National Laboratory, Los Alamos, NM 87545
63. A. Hasagawa, Nuclear Data Center, Japan Atomic Energy Research Institute, Tokai-mura, Naka-gun, Ibaraki-ken 319-11, Japan
64. R. N. Hwang, Argonne National Laboratory, Reactor Analysis Div., Bldg 208, Argonne, IL 60439
65. R. P. Jacqmin, DER/SPRC/LEPH, Batiment 230, Centre d'Etudes de CADARACHE, 13108 Saint Paul-lez-Durance, France
66. N. Janeva, Bulgarian Academy of Sciences, 72, Boul, Tzarigradsko shosse, Sofia 1784, Bulgaria
67. L. Lois, 08 E23, U.S. Nuclear Regulatory Commission, 11555 Rockville Pike, Rockville, MD 20852-2746
68. G. Leinweber, Gaertner LINAC Laboratory, Department of Environmental and Energy Engineering, Rensselaer Polytechnic Institute, Troy, NY 12180-3590
69. R. Little, X-TM, MS B226, Los Alamos National Laboratory, Los Alamos, NM 87545
70. C. Lubitz, Knolls Atomic Power Laboratory, P. O. Box 1072, Schenectady, NY 12301
71. R. E. MacFarlane, T-2, MS B243, Los Alamos National Laboratory, Los Alamos, NM 87545
72. C. Mounier, CEN Saclay, DMT/SERMA/LENR, 91191 Gif Sur Yvette Cedex, France
- 73-77. M. C. Moxon, 3 Hyde Copse, Marcham, Abingdon, Oxfordshire, England
78. D. Muir, IAEA Nuclear Data Section, Wagramerstr. 5, P. O. Box 100, A-1400 Wien, Austria
79. C. W. Nilson, Office of Nuclear Regulatory Research, U.S. Nuclear Regulatory Commission, Mail Stop TWFN 9-F-33, Washington, DC 20555
80. C. Nordborg, OECD/NEA, Le Seine St-Germain 12, Boulevard Iles, 92130 Issy-les-Moulineaux, France
81. C. Raepsaet, CEN Saclay, DMT/SERMA/LEPP, 91191 Gif Sur Yvette Cedex, France
82. M. Salvatores, DRN/P, Batiment 707, C. E. CADARACHE, 13108 Saint Paul-lez-Durance, France
83. E. Sartori, OECD/NEA, Le Seine St-Germain 12, Boulevard Iles, 92130 Issy-les-Moulineaux, France
84. O. A. Shcherbakov, Petersburg Nuclear Physics Institute, 188 350 Gatchina, Leningrad District, Russia
85. R. Shelley, Central Bureau for Nuclear Measurements, Steenweg op Retie, 2240 Geel, Belgium
86. K. Shibata, Nuclear Data Center, Japan Atomic Energy Research Institute, Tokai-mura, Naka-gun, Ibaraki-ken 319-11, Japan
87. R. Slovacek, Gaertner LINAC Laboratory, Department of Environmental and Energy Engineering, Rensselaer Polytechnic Institute, Troy, NY 12180-3590
88. A. B. Smith, Technology Development Division, D-207, AA115, Argonne National Laboratory 9700 South Cass Avenue Argonne, IL 60439
89. D. L. Smith, TD-207-DB116, Argonne National Laboratory, Argonne, IL 60544
90. H. Takano, Nuclear Data Center, Japan Atomic Energy Research Institute, Tokai-mura, Ibaraki-ken 319-11, Japan
91. J.J. Wagschal, Racah Institute of Physics, The Hebrew University of Jerusalem, 91904, Jerusalem, ISRAEL
92. H. Weigmann, Central Bureau for Nuclear Measurements, Steenweg op Retie, 2240 Geel, Belgium
93. C. Werner, Rensselaer Polytechnic Institute, Troy, NY 12180-3590
94. R. White, Lawrence Livermore National Laboratory, P. O. Box 808, Livermore, CA 94550
95. M. Williams, Nuclear Science Center, Louisiana State University, Baton Rouge, LA 70803